Shock Waves (2013) 23:381–398
DOI 10.1007/s00193-012-0426-3

ORIGINAL ARTICLE

Head on collisions of compressible vortex rings on a smooth solid surface

Effects of surface distance variation

R. Mariani · K. Kontis · N. Gongora-Orozco

Received: 27 October 2011 / Revised: 25 July 2012 / Accepted: 3 December 2012 / Published online: 25 January 2013

Abstract An experimental study has been conducted on the effects of distance variation on the impingement process of compressible vortex rings on a stationary solid wall. An experimental incident Mach number of 1.61 was used. Qualitative and quantitative studies compared the impingement and interaction flow characteristics of a compressible vortex ring with a stationary, solid, smooth surface at three distances: 1.66, 3.33, and 5.00 inner diameters. The three distances corresponded to an under-developed vortex ring (1.66 inner diameters), a vortex ring at its development threshold (3.33 inner diameters), and a fully developed one (5.00 inner diameters). Qualitative schlieren results showed that the surface distance affected the shock/vortex interaction process along with the impingement process of the vortex ring and the flow structure of its trailing jet. Quantitative data were extrapolated to evaluate the propagation velocity of the vortex ring prior to impingement. The boundary layer thickness was also estimated. Particle image velocimetry studies showed the main and secondary vortices to have opposite vorticity, with the magnitude of the vorticity of the secondary vortices being approximately half of that of the main vortex. Surface pressure results reveal the symmetrical properties of the impinging flow, along with a direct correlation between the maximum pressure measured at the instant the vortex ring impingement and an increase in surface distance.

Keywords Vortex ring · Surface impingement · Shock/vortex interaction · Compressible

Communicated by R. Bonazza.

The paper was based on work that was presented at the 28th International Symposium on Shock Waves, 17–22 July, 2011, Manchester, UK.

R. Mariani (✉) · K. Kontis · N. Gongora-Orozco
School of MACE, University of Manchester,
Manchester M13 9PL, UK
e-mail: raffaello.mariani@yahoo.co.uk

K. Kontis
e-mail: k.kontis@manchester.ac.uk

1 Introduction

Since the dawn of time, humankind has felt the presence of shock waves in nature through thunders and volcanic eruptions and, unable to understand them, have associated their occasionally destructive might to divinities such as Zeus and Jupiter in the Greek and Roman mythology, the Norse divinity of Thor, and the elusive Thunderbird in the Native North American culture. Through history, albeit unknowingly, humans have been able to generate shock waves via the cracking of a whip or the explosion of fireworks. It was the invention of the atomic bomb that brought back fear and respect towards the might of this natural phenomenon [1]. For research purposes, shock waves can be easily generated in a laboratory environment using shock-tubes where a pressure discontinuity is initially present. The disruption of this discontinuity initiates a series of waves that coalesce into a single compression wave travelling downstream [2]. In the presence of confining walls, it reflects from the surrounding surfaces producing high levels of blasts and reflections [3]. In an open-ended shock tube, upon exiting into the surrounding atmosphere, the moving shock wave transitions from a planar to a spherical shock waves and attenuates. The flow contained in the shock tube also exits, forming a shear layer with the external fluid. This shear layer is carried away and starts rolling to form a vortex ring [4].

Interesting work has been completed on the formation and generation of a free compressible vortex ring with little

attention being given to its impingement process on a stationary surface. As such, it can be interesting to have an initial overview of the work completed in incompressible flow, bearing in mind the differences in fundamental flow properties such as, for example, the absence of shock waves. Initial work was conducted by Boldes et al. [5] who looked at the phenomenon of temporary velocity variation of the vortex ring upon impingement, and Walker et al. [6] who studied the boundary layer formation and separation due to impingement introducing the concept of the "virtual image" of the vortex ring on the stationary surface. Lim et al. [7] experimentally showed that the vortex ring's induced velocity coupled with the no-slip condition at the wall leads to the development of a boundary layer directly below the vortex core. Due to an adverse pressure gradient, the boundary layer is forced to separate from the wall and roll up into forming secondary vortices of opposite vorticity which can also cause the primary vortex ring to rebound from the surface. These results were confirmed by Saffman et al. [8], who also demonstrated that the secondary vortex rings orbit around the primary one. Verzicco and Orlandi [9] showed that the vorticity in the radial direction, which is greater than the one in the vertical direction, is deforming the ring in the vertical axis. More recently, Naitoh et al. [10] completed an extensive study on the interaction of primary and induced vortices, the formation of finger vortices, and the presence of azimuthal instabilities during the process of radial expansion. Archer et al. [11] presented the impingement of a vortex ring as a sequence of three distinct phases: approach, slowing down, and expansion. Referring to the "virtual image" concept introduced by Walker et al. [6], the approach phase is when the ring is far enough from the surface for its motion to be unaffected by its presence, the slowing down phase begins when the influence of its "image" on the impinging vortex becomes significant, reducing the ring translational velocity and initiating the radial expansion, and the expansion phase is the pure radial stretching of the vortex ring which is highly influenced by the presence of its "image."

Very little work has been done on the subject of compressible vortex rings impinging on stationary surfaces. The topic has been approached only relatively recently by Minota [12], who focused his studies on the interaction of the shock wave with a vortex ring, experimentally showing that the shock wave behaves differently depending on the part of the vortex ring with which it interacts: the inner section, which interacted with the centre part of the vortex ring, was slowed down by it, while the outer section was diffracted by the vortex core. Similar results were obtained by Tokugawa et al. [13] and Szumovski et al. [14]. With respect to the impingement of a vortex loop on a surface, Minota et al. [15] showed that the most noticeable effects are the radial expansion of the vortex ring with the formation of a shear layer and vortices on the wall, and a separation bubble at the core of the impinging vortex ring and jet. Similar results were obtained by Szumovski et al. [14], who showed that to the impingement and subsequent radial expansion of the vortex loop corresponds a variation in surface pressure. The interaction amongst stationary objects, shock waves, and compressible vortex loops has also been studied at the University of Manchester by Kontis et al. [3,16,17], Mariani and Kontis [18], and Mariani [19]. These studies, also conducted at high incident Mach number values, showed that the shock wave is reflected from the plate impinging on the approaching vortex ring. The central part of the reflected shock wave is captured by the vortex ring and is intensified by the opposing high-speed flow, while the outer section is diffracted by the vortex core. Upon impingement, the vortical flow rapidly expands radially developing a boundary layer on the surface which slows down the flow and increases the pressure distribution on the plate. After some time, the boundary layer separates from the plate generating a series of secondary vortices. Recently, additional work has been conducted by Murugan and Das [20–23] on the subject of compressible vortex rings impinging on stationary surfaces. Their work, which evaluated the impingement of vortex rings at lower Mach number values, primarily focussed on the subject of the noise production associated with such phenomena.

With limited literature on the impingement on the subject of compressible vortex rings, the work on impinging underexpanded jets can be of help in understanding some of the flow features such as the formation of stationary shock waves over the surface. An initial comprehensive study was carried out by Ladenburg et al. [24], who summarised the work by Mach and Prandtl stating that the oblique shock system present in the jet is reflected by the jet boundary with a change in phase and that the resulting Mach reflection (MR) configuration is stationary rather than a transient non-stationary phenomenon. With the space race in full swing in the 1960s and the goal of landing on the moon and safely returning to Earth by the end of the decade, studies were completed by NASA on the effects of jet impingement on a flat surface in vacuum conditions with a high Mach number jet [25]. Three shock formations were found to exist based on the surface distance and pressure ratio. At close plate distances, a stand-off shock wave is formed close to the surface. With an increase in plate distance, the stand-off shock behaves similarly to a Mach disk and moves closer to the nozzle exit transitioning, at very large distances, to an oblique shock system in the jet with a normal shock at the plate surface. Further studies were completed by Lamont et al. [26] who characterised the flow into a highly complex mixture of subsonic and supersonic regions with interacting shocks and expansions regions in the jet. They also described the presence of a stagnation bubble with recirculation and separation of the boundary layer over the plate. This work was expanded by Henderson [27]

and Henderson et al. [28] by studying the effects that the impingement process has on the sound production.

As a summary, the topic of compressible vortex rings impinging on a stationary surface can be defined as the combination of three distinctive phenomena: shock wave diffraction and reflection, shock/vortex interaction, and vortex ring impingement. With the shock wave diffraction and reflection having been extensively investigated and being beyond the scope of the current study, it is the purpose of this research to focus on the impingement of a vortex ring on a solid surface including shock/vortex interactions as the processes can affect the vortex ring impingement, especially for the case of the surface at close distance from the shock tube exit.

The combination of the shock/vortex and wall/vortex interactions is of great interest for future applications such as space vehicle return lift-off or non-destructive weapons. It is the aim of the present study to enhance the knowledge in the field of shock wave and compressible vortex loops interaction with a stationary flat surface by evaluating the effects of the surface distance on their propagation and impingement.

2 The formation of a compressible vortex ring

Prior to presenting the study of an impinging vortex ring, it is useful to describe the formation and development of a free compressible vortex loop. This topic has been studied considerably both experimentally and analytically, and an extract of the available work is presented here. A good comprehensive description of the formation of a compressible vortex ring by means of a shock tube has been given by Baird [29] and Broadbent and Moore [4]. At the bursting of the shock tube diaphragm, a set of compression wave form and travel along the shock tube and set the fluid behind them to supersonic speed. These compression waves coalesce into a single shock front which, upon reaching the end of the shock tube, is expelled and diffracted by the exit edge. Fluid exiting the tube forms a shear layer with the external fluid, which is carried away and rolls up into a vortex. The flow in the shock tube behind the incident shock wave is accelerated by the expansion wave, and an underexpanded jet-like structure is formed, with the expansion wave forming attached to the shock tube's exit being immediately reflected by jet boundary with a shift in phase to an oblique shock wave. The oblique shock is reflected by its counterpart along the longitudinal axis of the flow as another oblique shock, resulting in a regular reflection-like structure. These sets of reflections are called shock-cells [24]. At Mach number greater than 1.43 [30], an embedded rearward-facing shock is formed, which extends between the internal core edges, and travels at the same propagation velocity of the vortex ring [12,29,31].

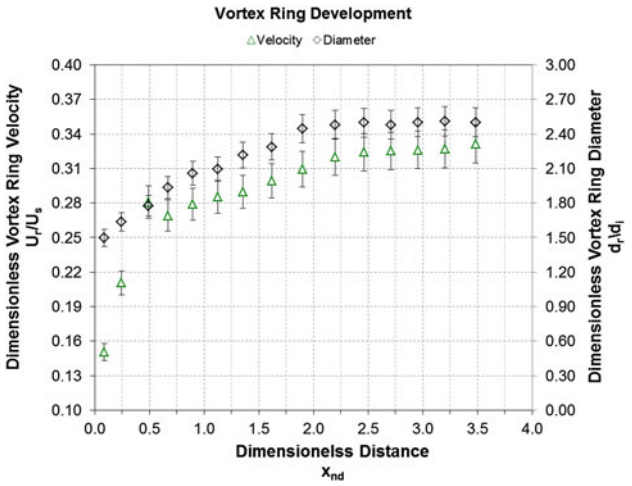

Fig. 1 Non-dimensional vortex ring propagation velocity and diameter growth

The strength of this shock wave increases with the increase in initial incidence shock wave Mach number. The velocity gradient along the embedded shock varies, increasing towards the vortex core, forming a strong shear layer ahead of it [32]. At Mach numbers $M > 1.6$, a set of counter-rotating vortex rings (CRVRs) form ahead of the main vortex structure. The mechanism for developing the counter-rotating vortex rings is similar to that of the generation of the main vortex ring, with the roll-up of the shear layer ahead of the embedded rearward-facing shock into vortices. The counter-rotating vortex rings move around the periphery of the main one, and has an opposite circulation with respect to it [16].

As the current study evaluates the impingement process of a vortex ring on a surface at different distances, it can be useful to plot the free vortex ring development in terms of non-dimensional propagation velocity and diameter growth to evaluate the "ideal" development of a free compressible vortex ring. These parameters are shown in Fig. 1. Data show that, at a distance from the shock tube of approximately $3.0d_i$, the vortex ring has reached a near constant maximum velocity and diameter. This is in good agreement with the work by Arakeri et al. [33], showing that such definition is also valid for vortex rings with the driver section of the shock tube set at the critical value. The vortex ring can, therefore, be considered under-developed at $1.66d_i$, at the development threshold at $3.33d_i$, and it can be assumed to be fully developed at $5.00d_i$.

3 Fundamentals of the impingement process of a compressible vortex ring on a surface

Prior to discussing the results, it is useful to give a short description of the fundamental characteristics of the impingement of a compressible vortex ring at high incident Mach

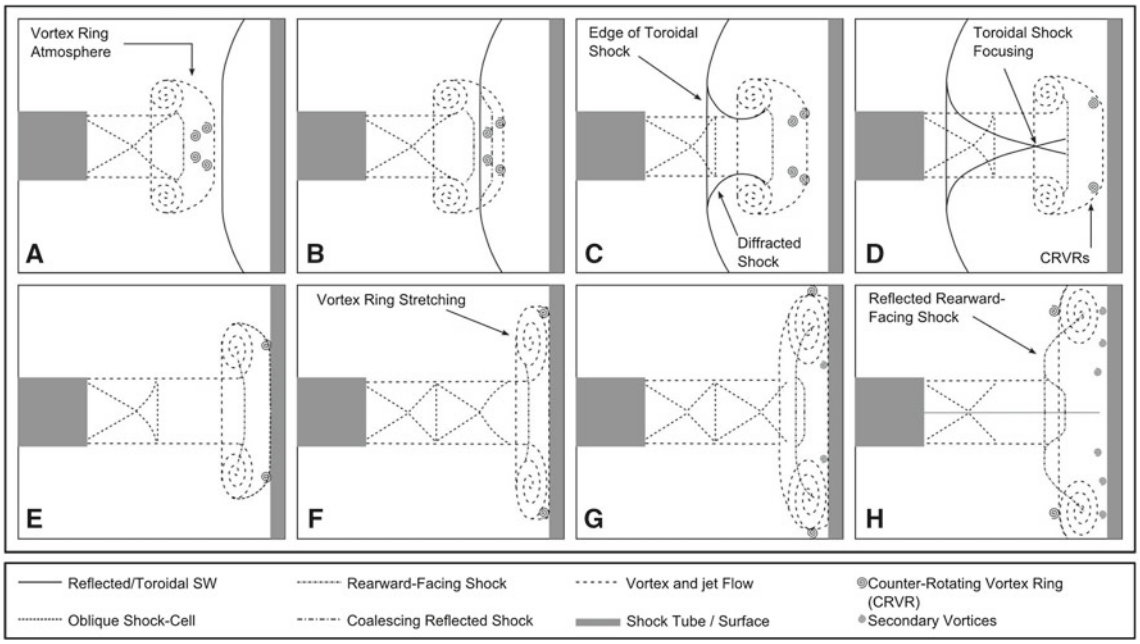

Fig. 2 Schematic example of the impingement process of a compressible vortex ring at high incident Mach number values on a stationary surface perpendicular to the flow propagation

numbers on a stationary surface perpendicular to the direction of propagation of the flow. The process is shown in Fig. 2.

The shock wave impinges on the surface and is reflected towards the approaching vortex ring (*A*), interacting first with the counter-rotating vortex rings (*B*). The centre section of the reflected shock wave begins to take a similar shape to that of the embedded rearward-facing shock (*B*) and, as the flow develops, it coalesces with it (*C*) [3]. Meanwhile, the outer section of the shock is being diffracted by the vortex core (*C*) [34], resulting in the outer section at each end of the shock wave travelling faster than the central part and rotating, becoming horizontal with the vortex ring central axis [35]. The combination of these two separate processes leads to the formation of a toroidal shock wave which focuses along the central longitudinal axis of the flow (*D*) [13].

Once the shock/vortex interaction process is completed, the vortex ring begins to impinge on the surface. The counter-rotating vortex rings impinge first (*D*) on the surface, simultaneously to the impingement of the atmosphere of the vortex ring. A boundary layer is formed over the surface by the approaching vortical system. The counter-rotating vortex rings begin to expand radially as the main vortex approaches the surface (*E*), undergoing a stretching process (*F*). The embedded rearward-facing shock inverts its curvature and is reflected by the flow over the surface (*G-H*). Secondary vortices of opposite rotation to that of the main one begin to be generated, expanding radially and orbiting around it, as the main vortex ring also expands radially (*H-F*). The reflected embedded rearward-facing shock is diffracted by the jet flow resulting in the formation of a second toroidal shock wave.

4 Experimental set up

4.1 Shock tube

Experiments have been carried out in a constant cross-section shock tube with an inner diameter (d_i) of 30 mm and outer diameter (d_o) of 38 mm. The driven section was open to ambient conditions and had a fixed length of 1,310 mm, while the driver section had variable length [36]. Air was used as both the driver and driven gas with a diaphragm pressure ratio P_4/P_1 of $\approx$12, producing a theoretical Mach number $M_1 = 1.66$. The shock tube was set-up with the driver section at its critical length, which is the length of the driver section required so that the reflected expansion fan generated upon rupturing of the diaphragm interacts with the incident shock wave at the exit of the shock tube [30]. The critical driver section length was calculated and set at 141 mm for the current experiment. The use of the critical length also ensures the reduction of disturbances and maximises the obtainable flow [2]. The diaphragm opening process also affects the flow within the shock tube with three-dimensional effects in the flow and requiring several shock tube diameters to fully form [2]. The disturbances and viscous effects inside the shock tube along with the diaphragm-opening process lead to the generation of an experimental Mach number $M_{se} = 1.61 \pm 0.03$, showing a repeatability error of $\sim$4 %.

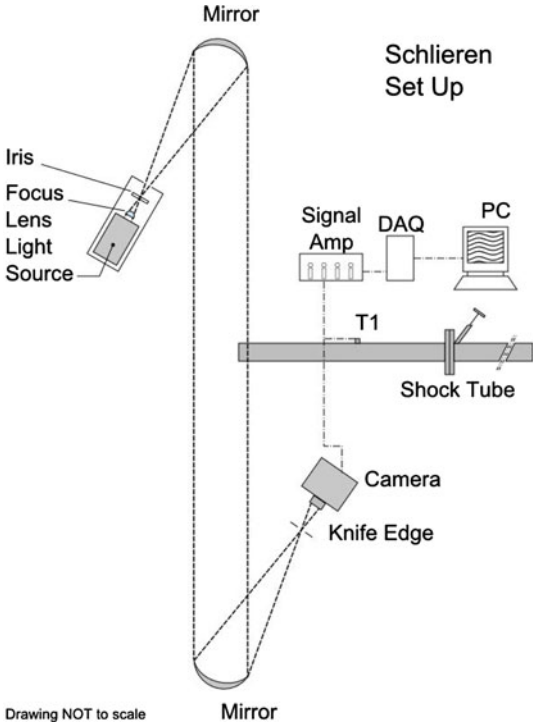

Fig. 3 Schematic diagram of the Schlieren set up

4.2 Schlieren set up

High-speed schlieren photography was employed to visualize the flow. The standard Z-type Toepler schlieren set up was the same as previously used at the University of Manchester [36]. The schematic is shown in Fig. 3. The light source was provided by a continuous 300W xenon lamp. The light beam passes through a plano-convex length of 90 mm in diameter and with a focal length of 90 mm. The focal point of the light is cut by a slit to regulate the amount of light available in the system. The light beam is collimated by a parabolic mirror of 203.33 mm diameter, f 4.5, and 1,016 mm focal length. The collimated light passes through the open test section area and is focused on a second parabolic mirror of equal diameter, focal length, and f number. A knife-edge is placed at the focal point of the second parabolic mirror to control the sensitivity of the schlieren system.

Images were collected using the Shimadzu HPV-1 Hyper Vision camera at a range of acquisition times between 800 and 3,200 μs, resulting in an acquisition rate ranging from 128 to 32 kfps. The repeatability of the schlieren experiment is determined by setting the same driver pressure, and having the same time delay output and acquisition speed. Repeatability was tested by taking multiple runs at the same experimental settings and the repeatability error of the shock wave and vortex ring position is found to be approximately 3 %.

4.3 Particle image velocimetry

Particle image velocimetry (PIV) is a minimally intrusive measuring technique well suited to studying unsteady phenomena. PIV is based on the measurement of the displacement of a field of particles transported by the fluid [37]. For the current study, a TSI high-speed high-repetition PIV system with a New Wave Research Pegasus laser was used in conjunction with a high frame-rate Photron APX RS camera. The capturing frequency for the images was set to 1500Hz with image pairs captured at time intervals of $\Delta t = 3\,\mu$s to best fit the propagation velocity of the vortex rings. A model 9306A TSI jet atomizer was used to generate oil droplet particles of size ∼1–1.5 μm with a relaxation time τ of 2.2 μs. Frame capturing was controlled by an external synchronizer. The system was triggered using a pressure transducer (T1) placed along the shock tube. Post-processing was completed using the double-correlation method with correlation zones of 32 × 32 pixels and interrogation areas set to maximize the pixel-per-millimetre ratio within the experimental area

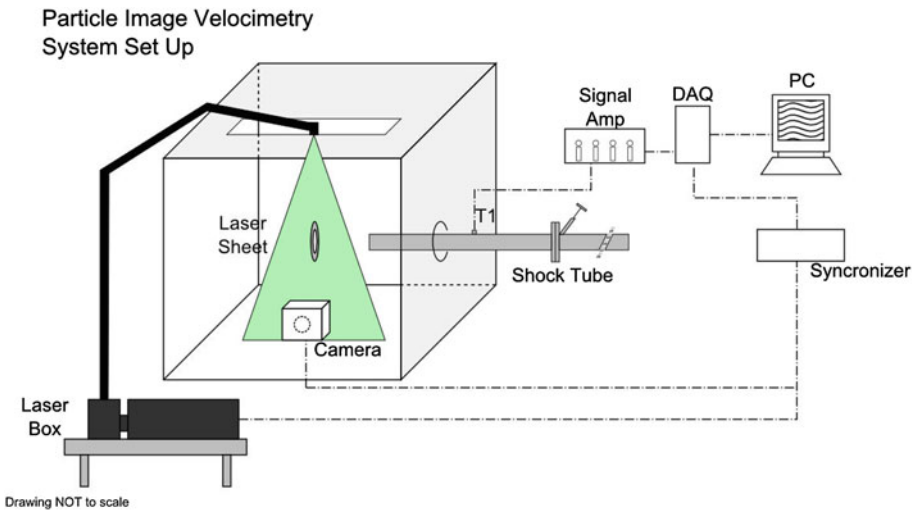

Fig. 4 Schematic of the PIV system

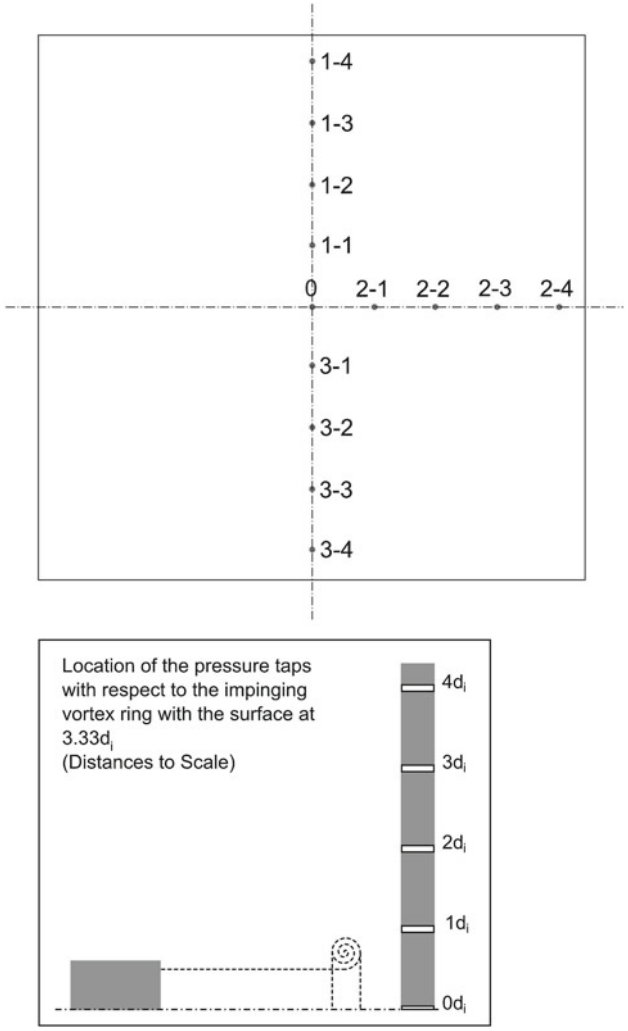

Fig. 5 Schematic of the pressure tap

of interest. Repeatability was tested by taking 3–5 runs at the same experimental settings and the repeatability error in the velocity field magnitude of the vortex ring is found to be approximately 3 %. A schematic of the PIV set up is shown in Fig. 4 [36].

4.4 Pressure measurements

The smooth surface was a squared aluminium plate 265 × 265 mm. Thirteen pressure taps (3 mm diameter) were drilled through the plate: one at the centre, and four aligned above, below, and to the right of the centre tap. The distance between each tap was 30 mm ($1.00d_i$). Five Kulite XT-190 transducers were mounted on the smooth surface along the same measuring line. The acquisition rate was 100KHz. The perpendicular and transversal acceleration sensitivity percentage of the transducer at 100 KHz is 1.5×10^{-3} and 2.2×10^{-4}. The five transducers were calibrated to an absolute pressure of 7 bar, with denser data towards the lower end of calibration curve. Figure 5 shows the schematic of the pressure tap configuration, where the first digit corresponds to the configuration number and the second digit to the tap number (i.e.: 1-3 means configuration 1 tap 3) along with the location of the pressure transducers with respect to the impinging vortex ring with the surface at the benchmark case of $3.33d_i$. The repeatability error is found to be between 3 and 5 %.

5 Results and discussions

In this experimental study, three surface distances were chosen: a benchmark case with surface placed at a distance of $3.33d_i$, a second case with surface at a distance of $1.66d_i$, and a third case with surface placed at a distance of $5.00d_i$

5.1 Benchmark case: $3.33d_i$

The first step in the current study was to study the benchmark case with the surface placed at $3.33d_i$ by repeating part of the experiments carried out at the University of Manchester by Kontis et al. [3]. Particle image velocimetry results have been added to the case, and pressure measurements aimed at also showing the symmetry in the process of impingement of the vortex ring on the surface.

5.1.1 Flow characteristics

The development of the impingement process of the vortex ring with the surface at $3.33d_i$ was evaluated and is shown in Fig. 6. In this instance, the reflected shock wave interacts first with the vortex rings train ($A-t = 0.408$ ms) causing an intensification of the vortex system [16]. The centre section of the reflected shock interacts and merges with the embedded rearward-facing shock, while its outer section is diffracted by the vortex core. In this experimental case, the shape of the shock wave interacting with the approaching vortex ring is curvilinear and the relative vortex direction with it is counter-clockwise. The diffracted shock wave continues to rotate generating a toroidal shock wave which diffracted sides converge on the central axis at the back of the vortex loop. In terms of vorticity magnitude, it is increased by the compressibility effects of the vortex [38]. Results suggest that the diffraction of the shock wave by the vortex is weak since the focusing of the resulting toroidal shock wave does not appear to affect the flow structure of the oblique shock system in the trailing jet. The vortex ring continues to propagate towards the surface with the CRVRs impinging first ($B - t = 0.504$ ms), and expanding radially as the main vortex fully impinges ($C - t = 0.648$ ms). The embedded rearward-facing shock transitions to a flat shape. An area of strongly compressed

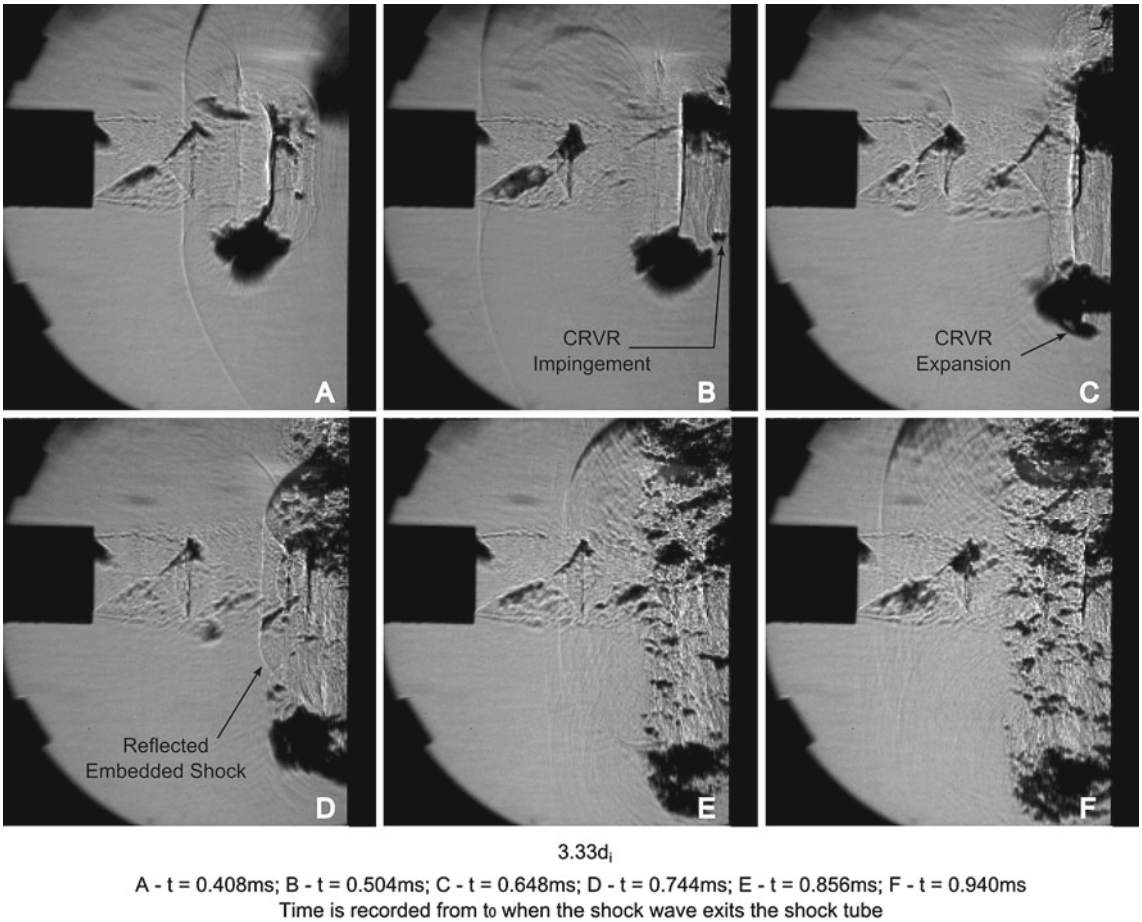

Fig. 6 Flow impingement process at a surface distance of 3.33dd_i

flow between the wall and the embedded shock wave is generated reflecting it ($D - t = 0.0.744$ ms). At this stage, a surface shock wave is formed ($E - t = 0.856$ ms), which is still visible during the formation of the secondary vortices linked to the development of a boundary layer on the surface, changing the pressure distribution along the wall ($F - t = 0.940$ ms) [3,16].

The flow field of the impinging vortex ring, both in terms of velocity magnitude and vorticity field, was evaluated quantitatively using the PIV system. Results indicate that the velocity of the radially expanding vortex ring is 200 ± 3.0 m/s, being approximately half of maximum found within the trailing jet flow of 380 ± 5.7 m/s. A shear layer is formed over the surface as a result of the induced velocity of the impinging vortex ring with the no-slip conditions at the boundary [7] and it decays in time. Results also show that the vorticity of the shear layer is approximately half of that of the impinging vortex ring. The vorticity field is shown in Fig. 7. The secondary vortices are shown to orbit around the primary one, as shown in Fig. 7. Results also indicate that there is a decrease in both velocity magnitude and vorticity with time, as shown in Table 1. The 3 % error is added to the velocity magnitude data, while the vorticity field is averaged over several locations along the main vortex ring and shear layer/secondary rings.

5.1.2 Wall pressure measurements

A wall pressure analysis was conducted to assess the distribution generated by the impinging shock wave and vortex ring on the surface. The pressure measurement also aimed at proving the symmetry of the impingement process. Three sets of discreet comparable data points were taken: one set above the centre point, one horizontal, and one below. A schematic of the plate is shown in Fig. 5. Tap 0, which is at the stagnation point of the impinging vortex ring and jet, was used to prove the repeatability of the set up which is shown in Fig. 8 (left). Symmetry is shown to occur across the plate in Fig. 8 (right), using the pressure plots at Tap 3 at 3.00d_i away from the centre. Time was normalised to facilitate data comparison. Pressure peaks measured at Tap 0 were found to compare well with previous experiments at the University of Manchester [3]. The acquisition rate was increased to more accurately capture the unsteadiness of the impinging flow.

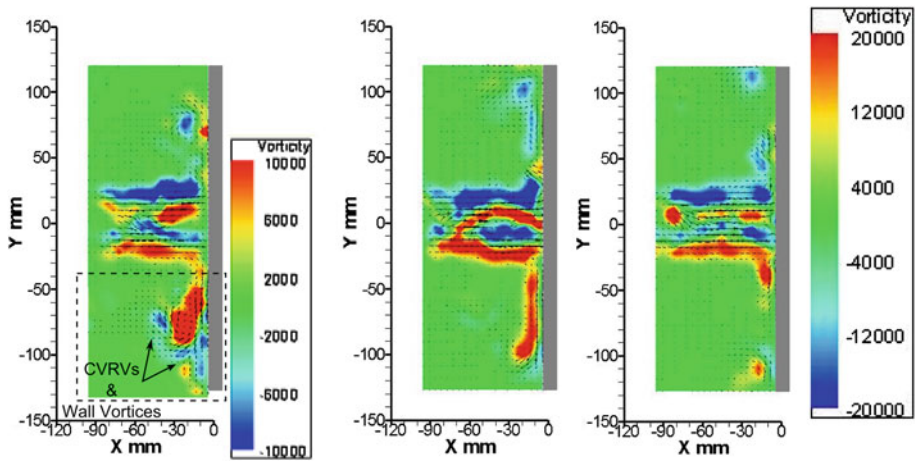

Fig. 7 Flow field of the impinging vortex ring at a surface distance $3.33d_i$ at time 0.578 ms (*left*), 0.978 ms (*centre*), and 1.244 ms (*right*)

Table 1 Velocity magnitude and vorticity of the main and secondary vortices with respect to time

Configuration	Time (ms)	Velocity (m/s)	Main ring vorticity	Secondary ring vorticity
	0.578	180 ± 2.7	$\pm$23,000	$\pm$9,000
$3.33d_i$	0.978	195 ± 2.4	$\pm$21,000	$\pm$8,000
	1.244	150 ± 1.8	$\pm$19,000	$\pm$6,000

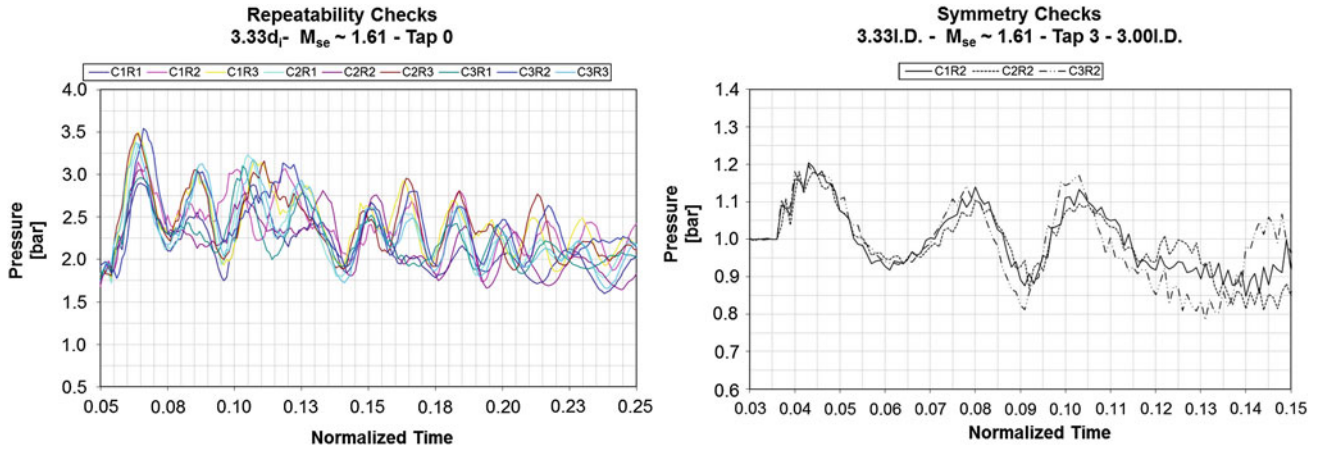

Fig. 8 Repeatability (*left*) and Symmetry (*right*) proof at the $3.33d_i$ surface distance case. In the legend C represents the configuration number and R the run number

After establishing repeatability and symmetry, the pressure variation along the plate was analysed in terms of the flow development. The pressure profiles can be separated into three distinct regions:

1. The impingement of the shock wave,
2. The maximum pressure peak of the vortex ring impinging followed by the fluctuation of the impinging jet flow,
3. The fluctuation and decay of the flow.

Figure 9 shows the pressure distribution along the plate plotted individually for each measuring location at the initial development prior to the beginning of the flow decay. As the impingement process was proven to be symmetrical, only one set of data is presented.

The flow development is described commencing from Tap 0, where the pressure variation is at its maximum. The first visible peak at $t = 0.032$ is due to the impingement of the shock wave on the surface, and is followed by a constant increase in pressure to a maximum value (1) of 3.43 bar at $t = 0.063$. The increase in pressure is caused by the adverse pressure gradient underneath the vortex core, forcing the boundary layer to separate. This process is also the direct cause for the formation of the wall vortices [39]. As the vortex ring impinges on the surface and it expands radially, the flow is accelerate and the pressure is reduced to a value of 2.29 bar (2). The flow then slows down again (3), before being increased by the formation of periodic secondary vortices over the surface (4). The periodic variation

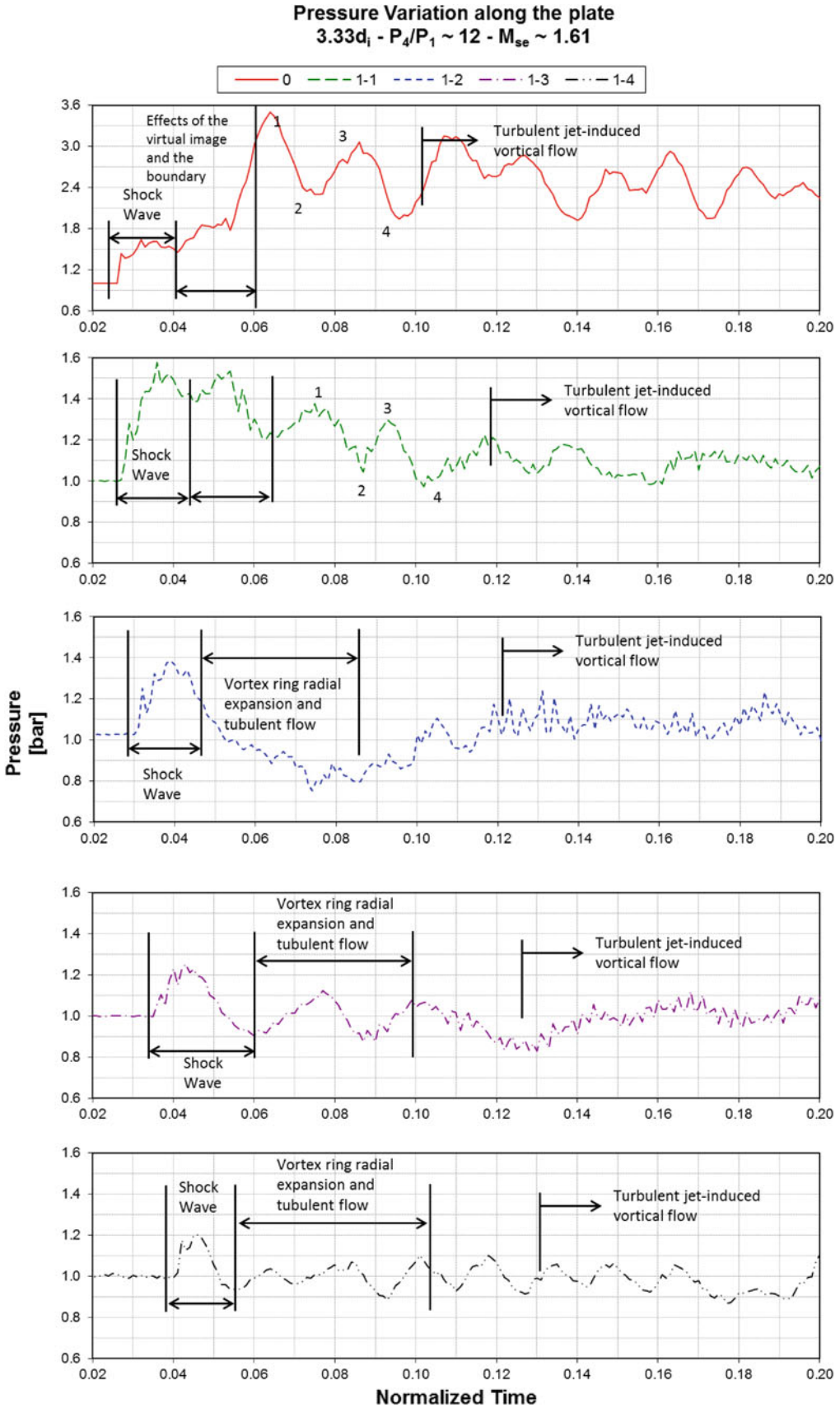

Fig. 9 Pressure variation along the plate at $M \sim 1.61$

in flow velocity results in the fluctuation of pressure values after the impingement of the primary vortex ring. These secondary vortices grow weaker in time as the flow loses strength, explaining the presence of the decaying fluctuating flow. The expansion of the vortex ring can be followed at Tap 1, but it becomes difficult to distinguish the peaks at locations Tap 2 to Tap 4 as the flow becomes increasingly more turbulent.

5.2 Effects of distance variation

After completing the benchmark case study, the surface distance was varied at locations where the vortex ring was not fully developed ($1.66d_i$) and where the full development was achieved with the vortex ring propagation velocity having previously reached a near constant value ($5.00d_i$). In this case, the counter-rotating vortex rings have completed their move along the periphery of the main vortex loop not affecting it any longer.

The first case evaluated is with the surface at a distance of $1.66d_i$ from the exit of the shock tube, and is shown in Fig. 10. Time is shown from the exit of the shock wave from the shock tube. The close proximity of the plate to the nozzle exit reduces the lag time between the interaction of the vortex ring and the reflected shock wave, which also is diffracted by the inner edges of the shock tube generating a pair of additional vortex rings. The counter-rotating vortex rings are still developing ($A - t = 0.288$ ms) and they impinge simultaneously with the main vortex ring, and both begin to expand radially. The initial propagation of the additional vortex rings is also visible. Flow visualization results in Fig. 10 showed that the shock-cell structure has been affected by the passing of the toroidal shock as it propagates through the jet. The deformation of the shock-cell structure indicates that the strength of the toroidal shock wave has increased compared to the results for the $3.33d_i$ case where the passing of the toroidal shock wave does not affect the shape of the shock cell. At $t = 0.328$ ms (B), the main vortex ring is expanding along the surface with the counter-rotating vortex rings being trapped in the central part of the flow. The downstream section of the shock-cell modifies into a bowed shape with the embedded rearward-facing shock becoming flat ($C - t = 0.368$ ms), and commencing to be reflected by the highly compressed flow between it and the solid plate. The first of the two additional vortex rings reaches the surface impinging on it. At $t = 0.408$ ms (D), the second, stronger, of the two additional vortex rings reaches the main vortical flow structure and interacts with the embedded rearward-facing shock. This shock/vortex interaction is in every respect similar to the main shock/vortex interaction, with the outer section of the shock being diffracted by the vortex ring core and the inner section being captured within the trailing jet structure ($E - t = 0.448$ ms and $F - t = 0.488$ ms). This process results in the formation of another toroidal shock wave. In the mean time, the main vortex ring continues to expand radially and secondary vortices are generated along the surface ($D - t = 0.408$ ms, $E - t = 0.448$ ms, and $F - t = 0.488$ ms). The flow on the surface is seen to be highly turbulent.

The surface was then moved farther away at a distance of $5.00d_i$, where the vortex loop is fully developed (Fig. 11). The reflected shock wave interacts first with an almost fully developed counter-rotating vortex ring ($A - t = 0.512$), and subsequently with the main vortex loop. The shock/vortex interaction is similar to the previously explained cases with the reflected shock wave inner section interacting with the embedded rearward-facing shock in the vortex ring and the outer section being diffracted by the vortex core. The main vortex loop continues propagating towards the stationary surface with the counter-rotating vortex rings having fully orbited around it prior to its impingement on the surface ($B - t = 0.672$ ms and $C - t = 0.768$ ms). Upon impingement of the vortex ring, the rearward-facing shock travelling within it is flattened ($D - t = 0.864$ ms), and is reflected by the highly compressed flow downstream. An oscillating surface shock wave is formed ($E - t = 0.992$ ms and $F - t = 1.152$ ms) to compensate for the pressure distribution on the surface.

5.2.1 Vortex ring impingement path

Quantitative data were extrapolated from the schlieren images to obtain the value of maximum linear propagation velocity of the vortex rings prior to impingement, to estimate the effects of the virtual image on the process, and the thickness of the boundary layer. Data are presented in non-dimensional form for the longitudinal propagation (x_{nd}), and radial expansion (y_{nd}). The shock tube inner diameter d_i was used as the non-dimensionalizing parameter. The impingement paths are shown in Fig. 12.

At the $3.33d_i$ benchmark case, the transition of the main vortex ring (M) from the linear propagation to the radial expansion results in an initially more gradual expansion, steepened when the counter-rotating vortex rings is not present downstream of the main vortex. The vortex ring reaches a maximum translational velocity $U_{r,x} \sim 152$ m/s at $x_{nd} = 2.6$, where it begins to be affected by its "virtual image," resulting in its deceleration. At the surface distance of $1.66d_i$, the vortex ring is almost immediately affected by the presence of the obstacle at $x_{nd} \sim 0.5$ with the maximum propagation velocity of 115.6 m/s achieved at $x_{nd} = 1.1$. When the surface distance is increased to $5.00d_i$, the vortex ring has a continuous gradual expansion from $x_{nd} = 1.39$ to $x_{nd} = 4.0$, within which length the counter-rotating vortex rings complete their move around the periphery of the main

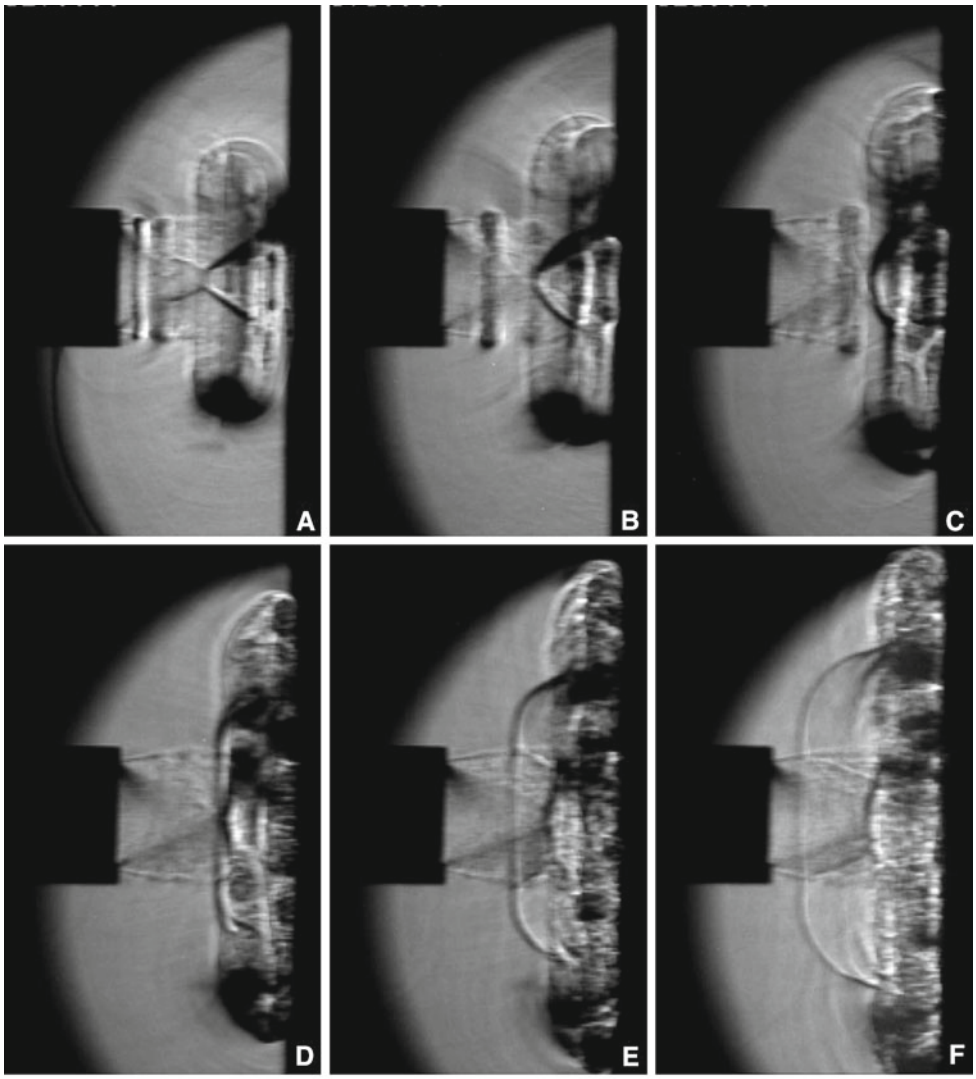

Fig. 10 Flow impingement process with a plate distance of $1.66d_i$

vortex. The maximum propagation velocity $U_{r,x}$ of 157 m/s is also achieved within this range of locations at $x_{nd} = 3.0$.

The path of the counter-rotating vortex rings and the additional secondary vortices (SV) has also been plotted. At $1.66d_i$ SV1, which corresponds to the first additional vortex generated by the diffraction of the reflected shock wave by the edges of the shock tube, is seen to reach a comparable value to the velocity of the main vortex ring, and decreases in size as it impinges on the surface. The reduction in size of SV1 suggests the occurrence of the phenomenon of leapfrogging, where the expanding secondary vortex over the surface acts as the leading ring, with the approaching ring decreasing in size and attempting to slip through it [36]. The second additional vortex rings (SV2) impinge and expand radially following the same trend of additional secondary vortices (SV) generated by the impingement of the trailing jet in the $3.33d_i$, suggesting that SV2 has an opposite rotational direction with respect to the main vortex ring. At the surface distance of $5.00d_i$, Fig. 12 shows that the CRVRs complete their orbiting motion around the main vortex ring M, prior to it impinging on the surface, with the secondary vortices SV1 and SV2 forming on the wall.

The maximum boundary layer thickness can be extrapolated from the graphs. Results show that the boundary layer thickness increases with an increase in surface distance, with a thickness of 11.7 mm at $1.66d_i$, 16.2 mm at $3.33d_i$, and 18.9 mm at $5.00d_i$. The increase in thickness is also visible in the particle image velocimetry flow field analysis. The increase in boundary layer thickness could be attributed to

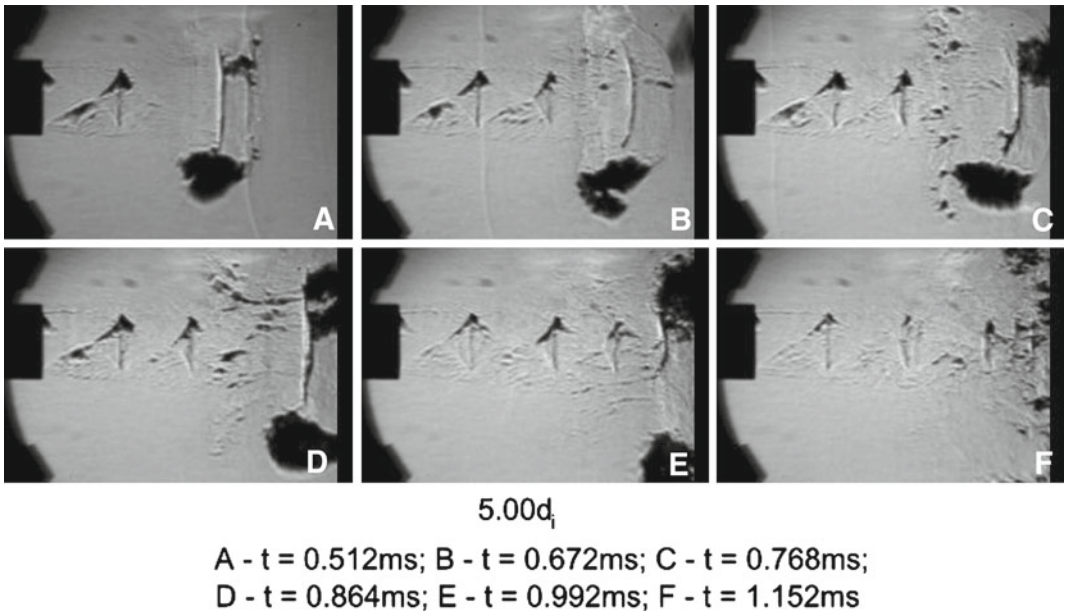

Fig. 11 Flow impingement process with a plate distance of 5.00d_i

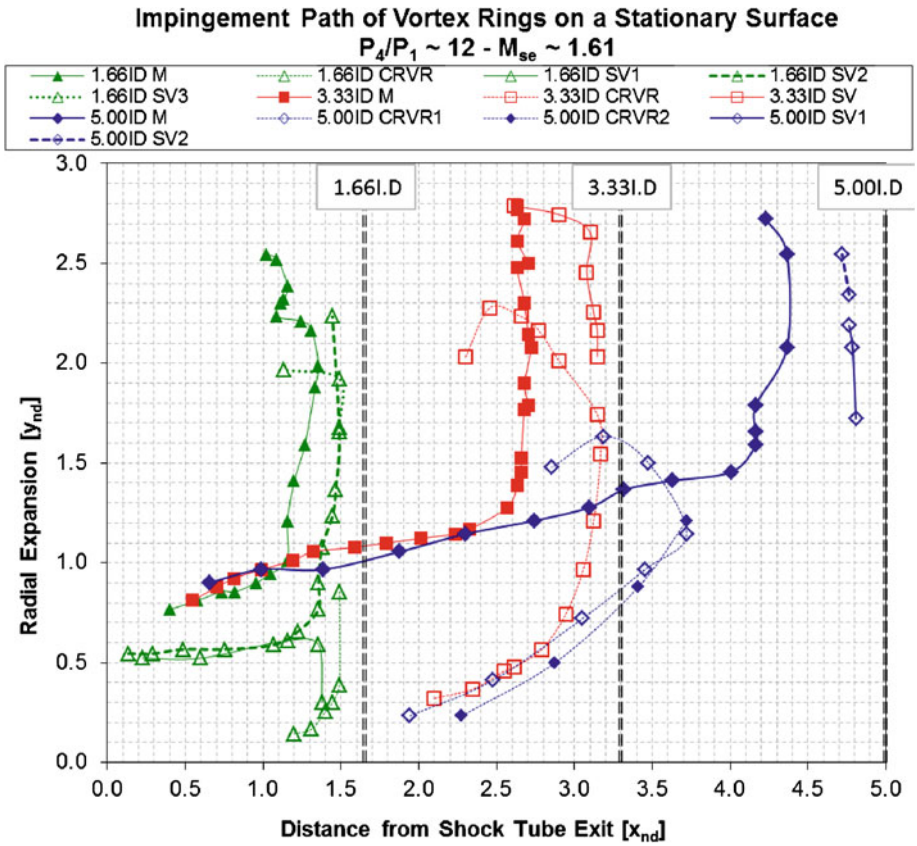

Fig. 12 Impingement path of a compressible vortex ring on stationary surfaces at distances of 1.66d_i, 3.33d_i, and 5.00d_i (*M* main vortex ring, *CRVR* counter-rotating vortex ring, *SV* secondary vortex, *1/2/3* first/second/third)

the larger size of the vortex ring as it is allowed to travel farther, as visible in the flow visualization, which also leads to the formation of a larger "virtual image".

5.2.2 Flow field

The flow field was evaluated in terms of the extrapolated velocity magnitude and vorticity field from the PIV plots. Results show that, when the surface distance from the shock tube exit is decreased to $1.66d_i$, there is an initial decrease in velocity magnitude and vorticity of the main vortex ring. With vorticity and flow velocity being closely related, it is reasonable that to a lower value of propagation velocity of the vortex ring corresponds a lower overall velocity magnitude and main vorticity at impingement. These results also agree with the extrapolated vortex ring propagation velocity. Simultaneously, the high-speed jet flow impinging on the surface delays the decay in radial velocity of the vortex ring. As the surface is moved farther away from the shock tube exit, both the velocity magnitude and vorticity field of the main impinging vortex ring increase. With respect to the vorticity level of the secondary vortices, it is again approximately half of that of the main vortex, and tends to remain relatively constant in value. As previously shown for the $3.33d_i$ case, both the velocity magnitude and vorticity field decay with time. The vorticity flow field of the two configurations is shown in Figs. 13 and 14 and presented in Table 2, with the data for the $3.33d_i$ case added for ease of comparison.

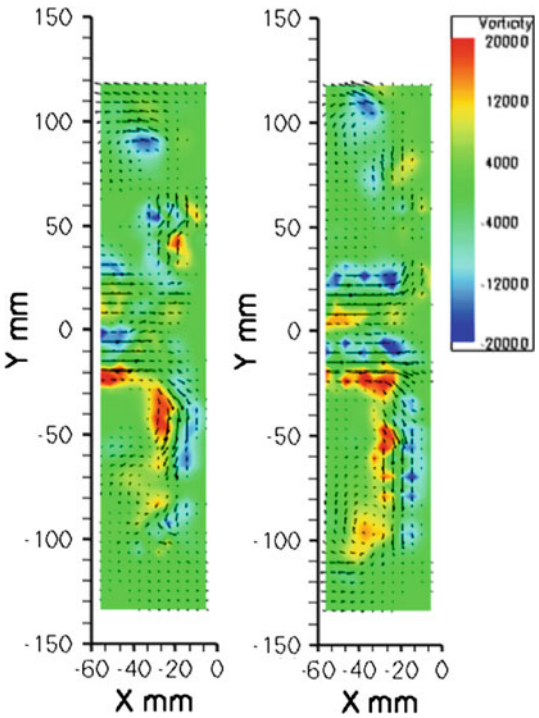

Fig. 13 Vorticity field characterization at $1.66d_i$ surface distance at time 0.420 ms (*left*) and 0.620 ms (*right*); recirculation bubble (*right*) characterization at $1.66d_i$ surface distance

Of additional interest in the flow characterization of the impinging vortex ring is the flow structure which results due to the close proximity of the shock tube exit to the surface. As shown in Fig. 15, a recirculation bubble is formed between the dome shock and the surface. The PIV study of the flow field shows that, while having a region of zero velocity at the very centre of the bubble region, the boundaries, which are formed by the shear layer between the main flow and the recirculation area, have a velocity magnitude in the range of 150 m/s. This value is comparable to the velocity magnitude over the surface, suggesting that the boundaries of the recirculation region undergo a similar radial acceleration as the main impinging flow. With respect to the vorticity field, the region is non-structured with an interchange of rotational direction starting from the most outer boundary. The vorticity field is shown to be in the region of ±10,000, a value lower than the main vorticity field of ±15,000. The recirculation bubble velocity magnitude and vorticity field characterization are shown in Fig. 15.

5.2.3 Wall pressure measurements

The wall pressure measurements shown in Fig. 16 were in good agreement with the flow field characteristics evaluated both qualitative and quantitatively. When comparing the results obtained at the three surface locations, the first outcome of the change in distance is the increase in the pressure magnitude of the impingement of the shock wave as the surface is moved closer to the shock tube exit. Oppositely, the maximum pressure peak of the developing boundary layer increases with an increase in surface distance. The increment in shock wave pressure is expected since at closer surface distances it is stronger, but the variation in boundary layer peak pressure is counter-intuitive.

As explained in Sect. 5.1.2, the maximum pressure peak is produced by the formation and separation of the boundary layer on the surface and, following the previous nomenclature, it is shown at positions 1–a–α. The pressure then decreases as velocity increases when the vortex ring rolls away (2–b–β). At the measurement locations farthest away from the centre of the surface, the pressure peaks corresponding to the vortex rings' impingement are not clearly defined due to the gradual decay of the flow during the expansion process. Results additionally show that at Tap 0 the time difference between each distinct initial pressure peak and drop with respect to the time of its corresponding maximum peak value is relatively constant regardless of the distance of the surface from the exit of the shock tube. As the vortex ring expands, it loses its compactness and symmetry making this behaviour at taps located farther from the centre less apparent.

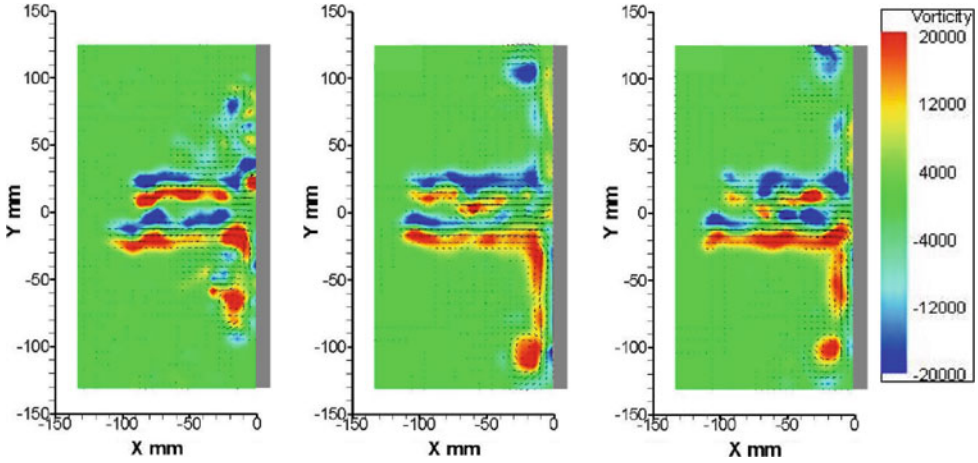

Fig. 14 Vorticity field characterization at $5.00d_i$ surface distance at time 0.920 ms (*left*), 1.120 ms (*centre*), and 1.220 ms (*right*)

Table 2 Velocity magnitude and vorticity of the main and secondary vortices with respect to time

Configuration	Time (ms)	Velocity (m/s)	Main ring vorticity	Secondary ring vorticity
	0.420	170 ± 5.1	$\pm$15,000	$\pm$12,000
$1.66d_i$	0.520	170 ± 5.1	$\pm$15,000	$\pm$10,000
	0.620	160 ± 4.8	$\pm$15,000	$\pm$10,000
	0.578	180 ± 5.4	$\pm$23,000	$\pm$9,000
$3.33d_i$	0.978	160 ± 4.8	$\pm$21,000	$\pm$8,000
	1.244	120 ± 3.6	$\pm$19,000	$\pm$6,000
	0.920	210 ± 6.3	$\pm$25,000	$\pm$11,000
$5.00d_i$	1.120	170 ± 5.1	$\pm$23,000	$\pm$10,000
	1.220	170 ± 5.1	$\pm$19,000	$\pm$10,000

Results suggest that there exists a correlation between the development stage of the impinging vortex ring and the boundary layer formation and separation, as well as with the additional parameter of the increase lag time between the shock wave and the vortex ring reflecting from the surface. The increase of the maximum peak pressure could be attributed to several factors in the flow, one of which being the value of the velocity of propagation at impingement, as the surface is moved away from the shock tube exit. At $M_{se} \sim 1.61$, the counter-rotating vortex rings ahead of the main vortex play a role in the initial variation in pressure distribution. The presence of the rapidly expanding counter-rotating vortex rings causes the transducer at Tap 0 to sense an acceleration due to their expansion, resulting in the presence of less stagnating fluid. This effect is mostly visible at the surface distance of $1.66d_i$, where the counter-rotating vortex rings are in their initial stages of development and the distance of the cores from Tap 0 is small (Fig. 10a). At this surface distance configuration, the counter-rotating vortex rings impinge between pressure Tap 0 and Tap 1-1, with the accelerated flow being sensed at that location as well as the counter-rotating vortex rings pass over it. As the distance of the surface is increased to $3.33d_i$, the location of the cores of the counter-rotating vortex rings at the moment of impingement is farther away from Tap 0, reducing the effects of the accelerated flow due to their presence on that pressure location as well as at Tap 1-1. At a distance of $5.00d_i$, the counter-rotating vortex rings are not present in the impingement process, and the flow is, therefore, allowed to stagnate at the moment of impingement prior to being deflected outwards, resulting in the increase in pressure shown in Fig. 16.

The force over the surface can be calculated associating with a defined area to each pressure tap. A square section of 30×30 mm with the pressure tap at its centre was chosen as the reference area. The forces are seen to increase with an increase in the distance of the surface from the exit of the shock tube. At Tap 0, this increase in the magnitude of the force is directly related to the structure of the vortex ring, in conjunction with the corresponding increase in pressure due to the stagnating flow over the surface as the distance of te surface from the exit of the shock tube is increased to $5.00d_i$. The pressure peaks and the corresponding instantaneous forces at the centre of the plate are presented in Table 3. As previously mentioned, at high incident Mach number value the flow rapidly becomes turbulent making it difficult to discern the

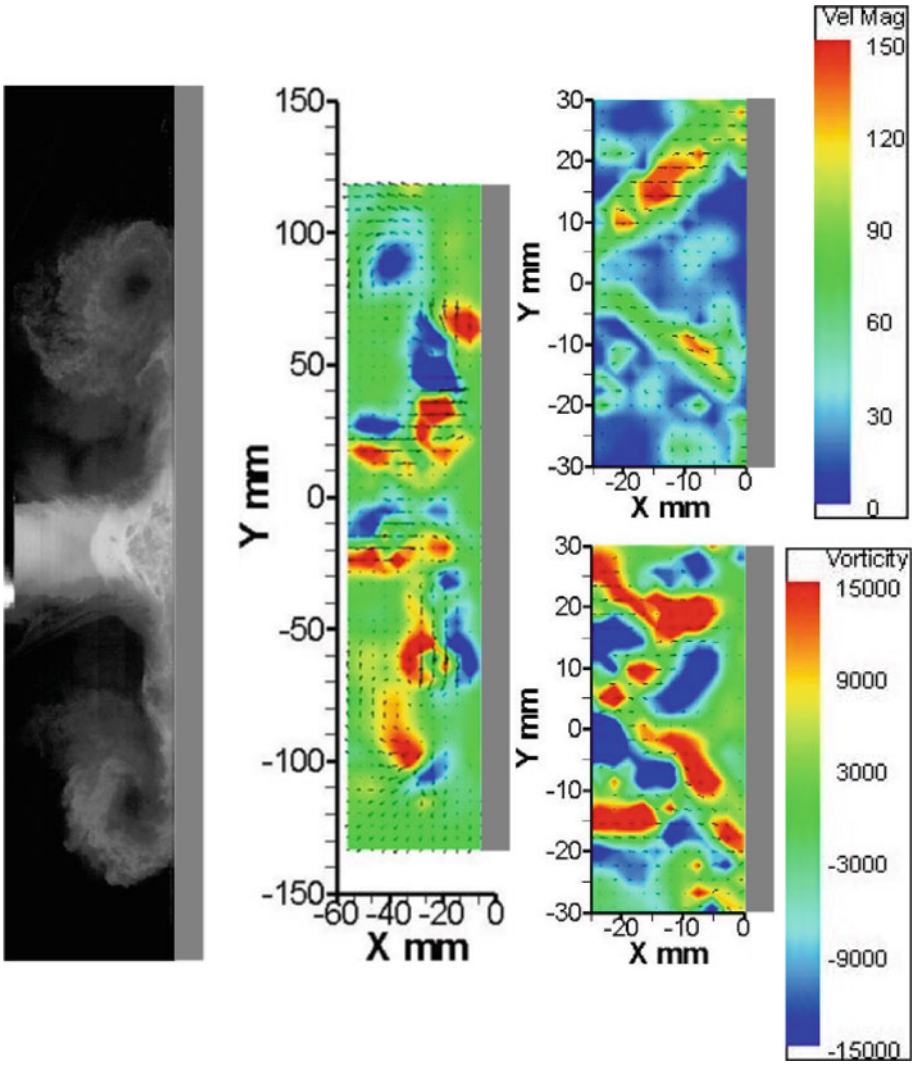

Fig. 15 Recirculation bubble characterization at $1.66d_i$ surface distance at time 0.520 ms; flow visualization (*left*), velocity magnitude (*top right*) and vorticity field (*bottom right*)

peak variations; therefore, only the stagnation pressure of the shock wave (P_{SW}), of the impinging vortex ring (P_{max}), and of the vortex ring at $1.00d_i$ (P_{T1}), are shown, along with the respective force measurements.

6 Conclusions

An experimental study was conducted evaluating the effects of the variation of the distance of a surface from the exit of the shock tube on the impingement process, flow field, and wall pressure distribution of an impinging vortex ring. Three distances were evaluated: $1.66d_i$, $3.33d_i$, and $5.00d_i$. Initially, a detailed benchmark experiment ($3.33d_i$) was carried out, confirming and also expanding the work completed by Kontis et al. [3]. The assumption of axisymmetric flow was proven to be acceptable despite the presence of the counter-rotating vortex rings, which inherently add some asymmetry in the flow.

Flow visualization of the benchmark case showed that the reflected shock wave has different interaction processes with the approaching vortex ring depending on the location of their interaction. The outer section of the shock wave is diffracted by the vortex core, while the central section is captured by the embedded rearward-facing shock at the centre of the vortex ring. The process results in the formation of a toroidal shock wave which focuses in the trailing jet along the longitudinal axis of the flow. The shock-cell structure within the jet does not appear to be affected by the shock wave focusing.

The extrapolation of the propagation data showed that the vortex ring reaches a maximum velocity of 152 m/s prior to being slowed down by the influence of its "virtual image." As the vortex ring approaches the surface, a boundary layer is generated and subsequently separates, resulting in a significant increase in pressure over the surface, to a maximum peak of 3.43 bar. The counter-rotating vortex rings are seen to impinge first. The pressure is decreased as the impinging vortex expands radi-

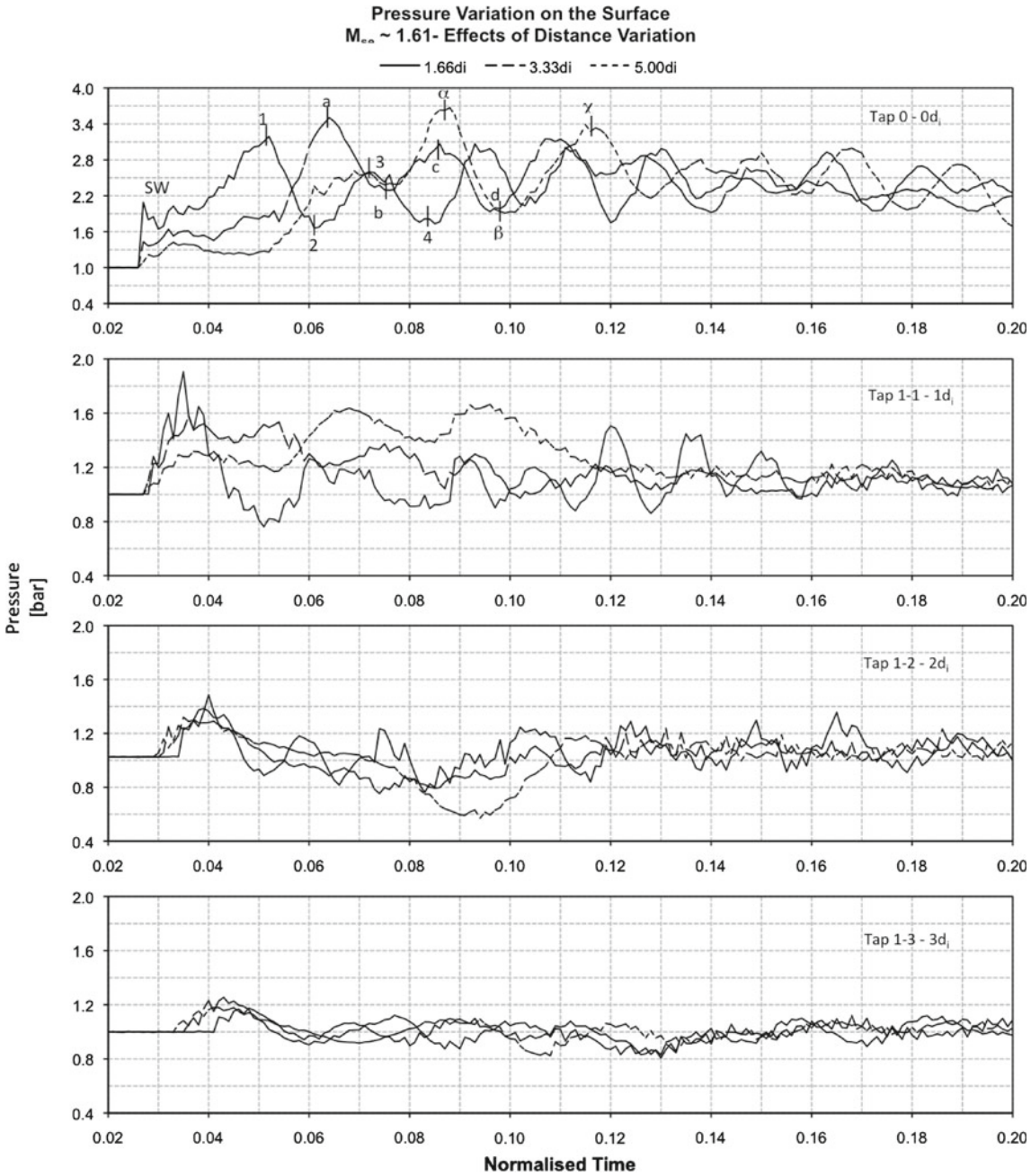

Fig. 16 Effects of the distance variation on the impingement of the incidence shock wave and vortex ring

Table 3 Effects of surface distance variation on the wall pressure at plate centre

Surface distance	P_{SW} (bar)	P_{max} (bar)	P_{T1} (bar)	F_{SW} (N)	F_{max} (N)	F_{T1} (N)
1.66	2.11	3.16	1.24	189	284	111
3.33	1.56	3.43	1.37	140	308	123
5.00	1.38	3.63	1.66	124	326	149

ally accelerating the flow. This process is followed by a periodic increase/decrease in surface pressure, as secondary vortex rings are generated and radially expand upon their impingement. The velocity magnitude and vorticity field of the expanding vortex ring were seen to decay with time.

The variation in surface distance leads to a significant variation in the flow features present at the moment of impingement of the vortex ring. As the surface is moved to $1.66d_i$, the resulting toroidal shock wave from the reflected shock/vortex interaction modifies the shock-cell structure within the trailing jet as it focuses along the longitudinal axis. Oppositely, as the distance is increased to $5.00d_i$, the reflected shock wave becomes weaker and, therefore, results in a weak shock/vortex interaction and does not affect the trailing jet structure.

At the surface distance of $1.66d_i$, the vortex ring is still at the beginning of the development stage, and it is almost immediately affected by the "virtual image." This situation results in the vortex ring reaching a smaller maximum translational velocity of 115 m/s, when compared to the experimental configurations. The counter-rotating vortex rings are at the very initial stages of their development as they impinge on the surface simultaneously with the main vortex ring. As the surface distance is increased to $5.00d_i$, the vortex ring has time to develop reaching a maximum translational velocity of 157 m/s. The counter-rotating vortex rings are also able to complete their move around the periphery of the main one, effectively not contributing to the impingement process. The velocity magnitude and vorticity field are also affected, both decreasing with a decrease in surface distance. The vorticity is seen to range from $\pm$15,000 to $\pm$25,000. With respect to the secondary vortices generated at the surface, vorticity data confirm the opposite direction with respect to the main vortex ring. The vorticity value of the secondary vortices is shown to being approximately half of that of the main vortex.

The extrapolation of data from the schlieren images, in conjunction with the particle image velocimetry results, has shown that there is an increase in boundary layer thickness over the surface with an increase in surface distance. The increase in boundary layer thickness can be attributed to the larger growth of the vortex ring as it is allowed to propagate farther prior to impingement, and the subsequent increase in the size of the "virtual image."

The pressure over the surface is also affected by the variation in surface distance. As expected, the shock wave impingement pressure decreased with an increase in surface distance as it becomes weaker during propagation. Oppositely, the maximum pressure peak increases with an increase in surface distance to a maximum of 3.63 bar at $5.00d_i$. The increase in pressure is thought to be due to the higher propagation velocity at impingement along with the position, or absence, of the counter-rotating vortex rings, and the increased presence of the stagnating flow. As the counter-rotating vortex rings impinge before the main vortex ring, their radial expansion causes a relative decrease in maximum pressure achieved, as it alters the boundary layer formation over the surface.

Acknowledgments The authors would like to acknowledge the financial support of the EPSRC-GB (Grant No. EP/E048498/1) and ESA-ESTEC (Grant No. 22692/09/NL/PA). The authors would also like to acknowledge Mr. Mark Quinn and Mr. Kinhing Lo, along with all the technical staff at the University of Manchester for their help in setting up the experiment. The support of the EPSRC loan pool in the person of Mr. Andrew Walker and of TSI instruments in the person of Dr. Martin Hyde is greatly appreciated.

References

1. Glass I.I.: Shock Waves and Man, edition, pp. 1–7. The Toronto University Press, Toronto (1974)
2. Gaydon, A.G., Hurle, I.R.: The Shock Tube in High-Temperature Chemical Physics, edition, pp 1–107. Chapman and Hall, London (1963)
3. Kontis, K., An, R., Zare-Behtash, H., Koundais, D.: Head-on collision of shock wave induced vortices with solid and perforated walls. Phys. Fluids **20**, 1–17 (2008)
4. Broadbent, E.G., Moore, D.W.: The interaction of a vortex ring and a coaxial supersonic jet. Proc. R. Soc. Lond. Ser. A Math. Phys. Sci. **709**, 47–57 (1987)
5. Boldes, U., Ferreri, J.C.: Behaviour of vortex rings in the vicinity of a wall. Phys. Fluids **16**(11), 2005–2006 (1973)
6. Walker, D.A., Smith, C.R., Cerra, A.W., Doligalski, T.L.: The impact of a vortex ring on a wall. J. Fluid Mech. **181**, 99–140 (1987)
7. Lim, T.T., Nickels, T.B., Ching, M.S.: A note on the cause of rebound in the head-on collision of a vortex ring With a wall. Exp. Fluids **12**, 41–48 (1991)
8. Saffman, P.G.: Dynamics of vorticity. J. Fluid Mech. **106**, 49–58 (1981)
9. Verzicco, R., Orlandi, P.: Vortex rings interacting with a wall. Appl. Sci. Res. **51**, 469–473 (1993)
10. Naitoh, T., Banno, O., Yamada, H.: Longitudinal vortex structure in the flow field produced by a vortex ring impinging on a flat plate. Fluid Dyn. Res. **28**, 61–74 (2001)
11. Archer, J.P., Thomas, T.G., Coleman, G.N.: The instability of a vortex ring impinging on a free surface. J. Fluid Mech. **642**, 79–94 (2010)
12. Minota, T.: Interaction of a shock wave with a high-speed vortex ring. Fluid Dyn. Res. **12**, 335–342 (1993)
13. Tokugawa, N., Ishii, Y., Sugano, K., Takayama, F., Kambe, T.: Observation and analysis of scattering interaction between a shock wave and a vortex ring. Fluid Dyn. Res. **21**, 185–199 (1997)
14. Szumovski, A., Sobieraj, G., Selerowicz, W., Piechna, J.: Starting jet–wall Interaction. J. Sound Vib. **232**, 695–702 (2000)
15. Minota, T., Nishida, M., Lee, M.G.: Shock formation by compressible vortex rings impinging on a wall. Fluid Dyn. Res. **21**, 139–157 (1997)
16. Kontis, K., An, R., Edwards, J.A.: Compressible vortex–ring interaction studies with a number of generic body configurations. AIAA J. **44**(12), 2962–2978 (2006)
17. Kontis, K., An, R., Zare-Behtash, H., Kounadis, D.: Head-on collision of shock wave induced vortices with a cylinder and a sphere. Int. J. Heat Fluid Flow **29**, 1380–1392 (2008)

18. Mariani, R., Kontis, K.: Head on collisions of compressible vortex loops on a solid wall effects of wall distance. In: Shock Waves, vol. 2, pp. 895–900. Springer, Germany (2012)
19. Mariani, R.: Compressible vortex rings and their interaction with stationary surfaces. Chap. 5, Thesis, The University of Manchester (2012)
20. Murugan, T., Das, D.: On the wall interaction of compressible vortex rings and associated noise. In: 37th AIAA Fluid Dynamic Conference and Exhibit, 25–28 June, Miami, Florida, AIAA-2007-3872 (2007)
21. Murugan, T., Das, D.: Propagation and wall interaction of compressible vortex ring: qualitative study. In: 9th Asian symposium on visualization, June 49, Hong Kong (2007)
22. Murugan, T., Das, D., Jain, M.: On the collision of compressible vortex ring with wall. J. Vis. **11**, 277 (2008)
23. Murugan, T., Das, D.: Characteristics of noise produced during impingement of a compressible vortex ring on a wall. Int. J. Aeroacoust. **9**, 815–824 (2010)
24. Ladenburg, R., Van Voorhis, C.C., Winckler, J.: Interferometric studies of faster than sound phenomena. Part II. Analysis of supersonic air jets. Phys. Rev. **76**, 662–677 (1949)
25. Vick A., Andrews, E.H. Jr., Winckler J.: An Investigation of Highly Underexpanded Exhaust Plumes Impinging Upon a Perpendicular Flat Surface. NASA Technical Note D-3269 (1966)
26. Lamont, P.J., Hunt, B.L.: The impingement of underexpanded axisysmmetric jets on perpendicular and inclined flat plates. J. Fluid Mech. **100**(3), 471–511 (1979)
27. Henderson, B.: The connection between sound production and jet structure of the supersonic impinging jet. J. Acoust. Soc. Am. **111**(2), 735–747 (2001)
28. Henderson, B., Bridges, J., Wernet, M.: Experimental study of oscillatory flow supersonic impinging jets. J. Fluid Mech. **542**, 115–137 (2005)
29. Baird, J.P.: Supersonic vortex rings. Proc. R. Soc. Lond. Ser. A Math. Phys. Sci. **409**, 59–65 (1987)
30. Brouillette, M., Hébert, C.: Propagation and interaction of shock-generated vortices. Fluid Dyn. Res. **21**, 159–169 (1996)
31. Minota, T.: Dynamic motion of a compressible vortex ring. Proc. SPIE **3173**, 241–248 (1997)
32. Murugan, T., Das, D.: Characteristics of counter-rotating vortex rings formed ahead of a compressible vortex ring. Exp. Fluids **49**, 12471261 (2010)
33. Arakeri, J.H., Das, D., Krothapalli, A., Lourenco, L.: Vortex ring formation at the open end of a shock tube: a particle image velocimetry study. Phys. Fluids **16**, 1008–1019 (2004)
34. Liang, S.-M., Ching, W.-T., Chen, H.: Numerical investigation of reflected shock/vortex interaction near an open end duct. AIAA J. **43**(2), 349–356 (2005)
35. Chatterjee, A., Povitsky, A.: Computational study of curved shock–vortex interaction. Int. J. Numer. Methods Fluids **30**, 257–277 (1999)
36. Mariani, R., Kontis, K.: Experimental studies on co-axial vortex loops. Phys. Fluids **22**, 126102 (2010)
37. Raffel, M., Willert, C.E., Wereley, S.T., Kompenhans, J.: Particle image velocimetry—a practical guide, edition. Springer, Berlin (2007)
38. Guichard, L., Vervisch, L., Domingo, P.: Two-dimensional weak shock–vortex interaction in a mixing zone. AIAA J. **33**, 1797–1802 (1995)
39. Green, S.I.: Fluid Vortices, edition, pp. 144–146. Springer, Berlin (1995)